Angewandte Chemie
Eine Zeitschrift der Gesellschaft Deutscher Chemiker

Supporting Information

Multi-Channel Lanthanide Nanocomposites for Customized Synergistic Treatment of Orthotopic Multi-Tumor Cases

Y. Liu, X. Zhu, Z. Wei, K. Wu, J. Zhang, F. G. Mutti, H. Zhang, F. F. Loeffler*, J. Zhou**

Materials and Methods

Materials: Rare-earth oxide Lu_2O_3 (99.999%) and Nd_2O_3 (99.99%) were purchased from STREM Chemicals Co. Ltd in USA. Oleic acid (OA) and indocyanine green (ICG) were purchased from Sigma Aldrich. NaOH, hydrochloric (HCl) solution, ethanol, cyclohexane, N,N-dimethylformamide, ethyl acetate and trichloromethane ($CHCl_3$) were purchased from Beijing Chemical Reagent Company. 1-octadecene, NH_4NO_3, and NH_4F were purchased from Alfa Aesar Chemical Co. Ltd. Tetraethyl orthosilicate (TEOS) was purchased from Aladdin Ind. Co. Hexadecyl trimethyl ammonium bromide (CTAB), (3-aminopropyl)triethoxysilane (APTES), N-hydroxysuccinimide (NHS), 1-(3-dimethylaminopropyl)-3-ethylcarbodiimide hydrochloride (EDC), reduced glutathione (GSH), L-buthionine sulfoximine (L-BS), and $(NH_4)_2MoO_4$ were purchased from Energy Chemical Co. Ltd. Doxorubicin was purchased from Adamas Reagent Ltd. GSH and GSSG assay kit was purchased from Beyotime Biotechnology. All bioreagent for cell culture and others were provided by Life Technologies Co., Ltd. Rare earth chlorides ($LnCl_3$, Ln: Lu and Nd) were prepared by dissolving the corresponding metal oxide in HCl solution at elevated temperature and then evaporating the water completely under reduced pressure. All other chemical reagents were of analytical grade and were used directly without further purification. Deionized (DI) water was used throughout.

Synthesis of $NaLuF_4$: Nd: The uniform $NaLuF_4$:Nd nanophosphor was synthesized by an optimized solvothermal method.[1] In a typical experiment, a mixture of 1 mmol $LnCl_3$ (Ln: 95%Lu, 5%Nd), 15 mL OA, and 15 mL ODE were added into a 100 mL

three-necked flask. Under the vacuum, the mixture was heated to 160 °C to form a clear solution, and then cooled to room temperature. After the solution had cooled down, 2.5 mmol NaOH (0.1 g) and 4 mmol NH_4F (0.1481 g) were added into the flask directly and stirred for 30 minutes. The solution was slowly heated under gentle stirring, degassed at 100 °C, and then heated to 300 °C and maintained for 1 hour under Argon atmosphere. After the solution had cooled down to room temperature (rt), the $NaLuF_4$:Nd nanoparticles were separated *via* centrifugation (10000 rpm) and washed with ethanol/cyclohexane (1:1 v/v) three times. The product was stored at rt in cyclohexane.

Synthesis of $NaLuF_4$:Nd@$NaLuF_4$: The coating of $NaLuF_4$ shell was performed by an optimized solvothermal procedure.[2] In a typical experiment, a mixture of 1 mM $LuCl_3$, 15 mL OA, and 15 mL ODE were added into a 100 mL three-necked flask. Under vacuum, the mixture was heated to 160 °C to form a clear solution, and then cooled to rt. After the solution cooled down, 0.025 mmol NaOH (0.1 g), 0.04 mmol NH_4F (0.1481 g), and as-prepared $NaLuF_4$:Nd nanoparticles were added into the flask directly and stirred for 30 minutes. The solution was slowly heated under gentle stirring, degassed at 100 °C, and then heated to 300 °C and maintained for 1 hour under the Argon atmosphere. After the solution cooled to rt, the $NaLuF_4$:Nd@$NaLuF_4$ were separated *via* centrifugation (10000 rpm) and washed with ethanol/cyclohexane (1:1 v/v) three times. The product was stored at rt in cyclohexane.

Synthesis of Ln-mSi: The mesoporous SiO_2 shell was coated by a typical Stöber method.[3] In a typical experiment, 250 μL $CHCl_3$ containing 5 mg as-prepared

$NaLuF_4$:Nd@$NaLuF_4$ were mixed with 2.5 mL CTAB solution (37.5 mg mL^{-1}) under sonication for 5 minutes. The mixture was transferred to a 100 mL three-necked flask and heated in a 60 °C water-bath to form a clear solution. Then, 22.5 mL DI water was added and the solution was heated to 70 °C before 0.3 mmol NaOH (0.012 g) was added directly. After 20 minutes stirring under stirring (600 rpm), 90 μL TEOS was added slowly and 0.5 mL ethyl acetate was added within 30 seconds. Finally, the solution was continuously stirred in a 70 °C water-bath for another 3 hours to enhance the stability of the $mSiO_2$ shell. After the solution was cooled to rt, the Ln-mSi were separated *via* centrifugation (8000 rpm) and washed with ethanol and DI water three times, respectively. The as-obtained nanoparticles were then suspended in 50 mL ethanol containing 0.3 g NH_4NO_3 upon stirring for 1 hour at 60 °C. The CTAB-removed Ln-mSi were separated *via* centrifugation (8000 rpm) and washed with DI water three times. The final product was stored at 4 °C in PBS.

Synthesis of Ln-mSiMo: In a typical experiment, 1 mL HCl solution was added to 5 mL DI water containing 5 mg as-prepared Ln-mSi. After stirring under room temperature for 10 minutes, 0.05 mmol $(NH_4)_2MoO_4$ (0.0098 g) was added directly and another 30 minutes was needed for stable modification. The Ln-mSiMo were separated *via* centrifugation (8000 rpm) and washed with DI water three times. The final product was stored at 4 °C in PBS.

Synthesis of Ln-mSiMo-dox: In a typical experiment, 20 mg Ln-mSiMo was dispersed in 10 mL DI water. Then, 5 mL aqueous solution containing the desired concentration of doxorubicin was added into the Ln-mSiMo suspension. After 4 or 12 h of gentle

stirring, the Ln-mSiMo-dox suspension was separated via centrifugation and washed with DI water for several times and stored at 4 °C in PBS.

Synthesis of Ln-mSi-ICG-dox: In a typical experiment, 30 mg Ln-mSi dispersed in 30 mL of ethanol in 100 mL flask and 0.3 mL of APTES was added. Afterwards, the reaction vessel was placed in 80 °C water boiling and refluxed for 12 h. The Ln-mSi-NH_2 was acquired by centrifugation and washed with ethanol and water several times, respectively. Then, the Ln-mSi-NH_2 was dispersed in 4 mL N,N-dimethylformamide solution containing 20 mg of EDC and 4 mg NHS. 3.5 mg ICG was dissolved in 1 mL of N,N-dimethylformamide, then added dropwise to the reaction vessel, and the solution was stirred for 12 h at rt. The Ln-mSi-ICG was obtained by centrifugation and was washed with methanol until the supernatant was colorless and stored at 4 °C in methanol. The Ln-mSi-ICG-dox were obtained with similar procedure as the Ln-mSiMo-dox and stored at 4 °C in PBS.

Characterization: The sizes and morphologies of $NaLuF_4$:Nd, $NaLuF_4$:Nd@$NaLuF_4$, Ln-mSi, and Ln-mSiMo were determined using a FEI Tecnai G^2F30 transmission electron microscope (TEM). Samples of the above nanoparticles were deposited on the surface of a copper grid. Energy-dispersive X-ray analysis mapping and scanning transmission electron microscopy (STEM) of the samples were also performed during TEM measurements. The size distribution was counted and calculated from TEM images (α = 0.90, 500 particles were measured). UV-vis-NIR absorption spectra were obtained on a Shimadzu UV-3600 UV-vis-NIR spectrophotometer. Powder X-ray diffraction (XRD) pattern was measured with a Brucker D8 advance X-ray

diffractometer from 10° to 70° (Cu Kα radiation, λ = 1.54 Å). Electrochemical measurements were conducted on a CHI-832 electrochemical workstation (Chenhua Instruments Co.). A three-electrode system was made up of a glassy carbon electrode (GCE, 4 mm in diameter) as the working electrode, an Ag/AgCl electrode (saturated KCl) as reference electrode, and a Pt wire as counter electrode. Nitrogen adsorption-desorption isotherms were recorded on a 3H-2000PS1 specific surface & pore size analysis instrument from BeiShiDe company. Before measurement, the sample was degassed at 90 °C in vacuum for 5 h. Fourier transform infrared spectra were measured using a Shimadzu Fourier Transform Infrared Spectrophotometer IRPRESTIGE-21 from samples in KBr pellets. The specific surface area was calculated using Brunauer–Emmett–Teller (BET) method, the pore size distribution was derived from the adsorption branch of the isotherm based on Barrett–Joyner–Halanda (BJH) model. Dynamic light scattering and zeta potential experiments were carried out on an ALV-5000 spectrometer goniometry equipped with an ALV/LSE-5004 light scattering electronic and multiple tau digital correlator and a JDS Uniphase He–Ne laser (632.8 nm) with an output power of 22 mW. The hydrodiameter distribution was measured at 25 °C with a detection angle of 90°. The fluorescence spectra were taken on a FLS980 lifetime and steady state spectrometer (Edinburgh Instruments). Fluorescence images were collected by a self-developed small animal fluorescence imaging system equipped with Andor iXon Ultra EMCCD (Si-based CCD) and Princeton Instrument NIRvana 640 CCD (InGaAs-based CCD) camera, as well as an external 0-8 W adjustable CW infrared laser (Hide-Wave Co., China). NIR I and NIR II

fluorescence images were collected by an InGaAs CCD using a 900 ± 10 nm bandpass and a 1064 ± 20 nm bandpass filter, respectively. NIR II/NIR I image and signal intensity were obtained by analysing NIR II and NIR I images using professional software provided by Andor. Photothermal temperature curves and thermal images were determined by a self-developed temperature determination system equipped with a thermocouple thermometer and a NIR camera (FLIR E40). Biomimic tissue phantoms were synthesized by a typical protocol by using sodium azide and gelatin.

Cell culture: Mouse breast cancer cell lines (4T1 cell line) were provided by the Institute of Basic Medical Sciences, Chinese Academy of Medical Sciences. Cells were grown in DMEM (Dulbecco's modified Eagle's medium), supplemented with 10% FBS (fetal bovine serum) and 1% penicillin-streptomycin at 37 °C with 5% CO_2. Cultures were maintained at 37 °C under a humidified atmosphere containing 5% CO_2.

MTT assays: 4T1 cells (90 μL $well^{-1}$, 10^5 cells mL^{-1}) were seeded into a 96-well cell culture plate, and the cells were incubated at 37 °C under 5% CO_2 for 24 h. Medium of Ln-mSiMo-dox (10 μL $well^{-1}$, containing 1% PBS) at mass concentrations of 0–5 mg mL^{-1} and different GSH concentrations of 100–900 μM were added to the wells, respectively, and medium containing 1% PBS (10 μL $well^{-1}$) was set as a control group. The cells were incubated at 37 °C under 5% CO_2 for 12 and 24 h, respectively. Subsequently, 3-(4,5-dimethylthiazol-2-yl)-2,5-diphenyltetrazolium bromide (MTT, 10 μL, 5 mg mL^{-1}) was added to each well of the 96-well assay plate and incubated for an additional 4 h. After the addition of dimethyl sulfoxide (DMSO, 100 μL $well^{-1}$), the assay plate was allowed to stand at room temperature for 30 min. A Tecan Infinite

M200 monochromator-based multifunction microplate reader was used to measure the OD570 (*Abs* value) of each well with background subtraction at 570 nm. A well without MTT was used as blank control. The following formula was used to calculate the viability of cell growth: Cell viability (100%) = (mean of *Abs.* value of treatment group - mean of *Abs.* value of blank)/mean *Abs.* value of control × 100%.

Hematology studies. All animal procedures were performed in accordance with the Guidelines for Care and Use of Laboratory Animals of Beijing Vital River Laboratory Animal Technology Co., Ltd. and approved by the Animal Ethics Committee of the Vital River Institutional Animal Care and Use Committee. The blood samples were harvested from mice intravenously injected with Ln-mSiMo (n = 3, dose = 20 mg kg^{-1}, Test) and from mice receiving no injection for 1 day, 7 days, 15 days, 30 days, and 60 days post-injection (n = 3, dose = 0 mg kg^{-1}, Control), respectively. The body weight of mice was also recorded. Blood was collected from the femoral vein. Five important hepatic indicators (ALT, alanine aminotransferase; AST, aspartate amino transferase; TBIL, total bilirubin; ALB, albumin; TP, total protein) and one indicator for kidney functions (CREA, creatinine) were measured. Blood smears were prepared by placing a drop of blood on one end of a slide, and using another slide to disperse the blood along the length of the slide.

Tumor xenografts. 4T1 cells were collected by incubation with 0.05% trypsin-EDTA. Cells were collected by centrifugation and resuspended in sterile PBS. Cells (10^8 cells per site) were orthotopically implanted into both, left and right breasts of 4-week-old female athymic Balb/c mice (m = 20 ± 2 g). All imaging and therapy were performed

when both tumor volumes reached ~60 mm^3.

Modulating intratumoral GSH level: 10 μL PBS solution containing L-BSO (1 mM) was intratumorally injected in the tumor of mice.[4] After 12 and 48 h post-injection, mice with medium and low intratumoral GSH level were obtained, respectively (Supplementary Fig. 7). To assess the intratumoral GSH level in various cases, tumors were collected from mice and GSH was extracted in each case by standard protocol. The intratumoral GSH level was determined by the GSH assay kit.

In vivo fluorescence imaging: In vivo fluorescence imaging was performed with a modified *in vivo* fluorescence imaging system using an external 0–8 W adjustable CW infrared laser (808 nm, Hide-Wave Co., China) as the excited source. Bright field images were collected by Andor iXon Ultra EMCCD. NIR I and NIR II signals were collected by Princeton Instrument NIRvana 640 InGaAs CCD. Images of signals were analyzed with corresponding software. 4T1 tumor-bearing nude mice (m = 20 ± 2 g) were anesthetized with 10% chloral hydrate (150 μL) and fixed by dual adhesive tape. Then, they were intravenously injected with PBS solution with and without of Ln-mSiMo-dox (10 mg kg^{-1}). The organs were harvested and thoroughly washed to remove residual blood. Next, NIR II fluorescence imaging was performed with the harvested organs, including stomach, intestine, kidney, tumors, liver, spleen, and lung. At various post-injection time points, whole-body imaging was performed. Ln-mSi-ICG-dox was also used for comparison.

In vivo photothermal imaging: 4T1 tumor-bearing nude mice (m = 20 ± 2 g) were anesthetized with 10% chloral hydrate (150 μL) and fixed by dual adhesive tape. Then,

they were intravenously injected with PBS solution with and without of Ln-mSiMo-dox (10 mg kg^{-1}) and irradiated by a continuous-wave diode NIR laser with a center wavelength of 808 nm and external output power intensity (0-1.5 W cm^{-1}) for 3 min. The temperature was measured by a digital thermometer with a thermocouple probe every 0.133 s. The photothermal images were obtained using FLIR E40 equipment running on FLIR tools systems.

Customized synergistic therapy in vivo. For customized photothermal therapy, all ten mice received intratumoral injection of Ln-mSiMo-dox (10 μL, 500 μg mL^{-1}). At 60 min after post-injection, fluorescence imaging was performed to each of the mice and, on the basis of calibration diagrams established in cell experiment, customized prescriptions were established for each tumor in the mice. Within the therapeutic process, mice were anesthetized and received whole-body irradiation by using the ring-shape laser array designed by our own group (Figure S13). The tumor sizes were measured by a caliper after treatment and calculated according to the formula: Tumor volume = (tumor length) × (tumor width)^2/2. The groups with same composition of mice and Ln-mSiMo-dox administration, irradiated by high laser power intensity for long irradiation time (0.75 W cm^{-2}, 180 s, *Abbr.* uniform high irradiation group) or by low laser power intensity for short irradiation time (0.15 W cm^{-2}, 60 s, *Abbr.* uniform low irradiation group), served as control groups. Ln-mSi-ICG-dox was also used for comparison. Ln-mSiMo with laser irradiation and Ln-mSiMo-dox without laser irradiation were used to demonstrate the synergistic effect of photothermal therapy and chemotherapy.

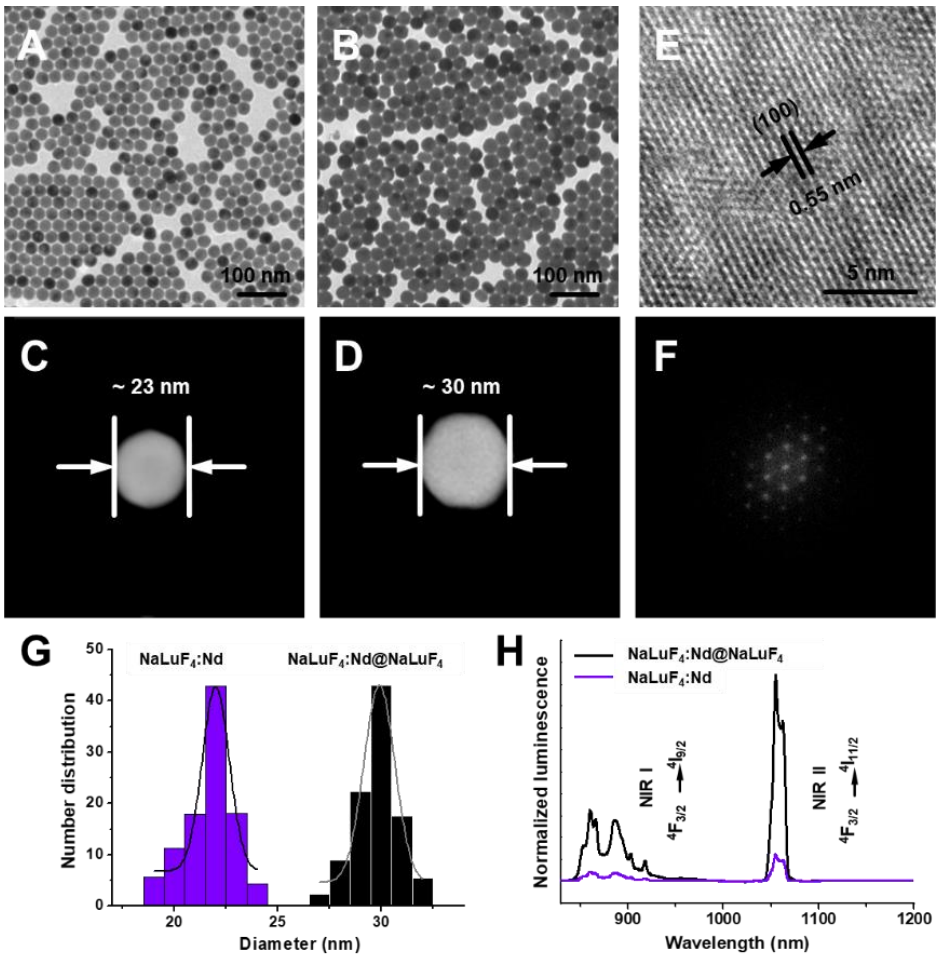

Supplementary Figure 1. Morphology and fluorescence properties of $NaLuF_4$:Nd and $NaLuF_4$:Nd@$NaLuF_4$. Transmission electron microscopy images of $NaLuF_4$:Nd (A) and $NaLuF_4$:Nd@$NaLuF_4$ (B). Scanning transmission electron microscopy images of $NaLuF_4$:Nd (C) and $NaLuF_4$:Nd@$NaLuF_4$ (D). High-resolution transmission electron microscopy image (E) and fast Fourier transformed image (F) of $NaLuF_4$:Nd@$NaLuF_4$. Diameter distribution (G) and fluorescence spectra (H) of $NaLuF_4$:Nd and $NaLuF_4$:Nd@$NaLuF_4$.

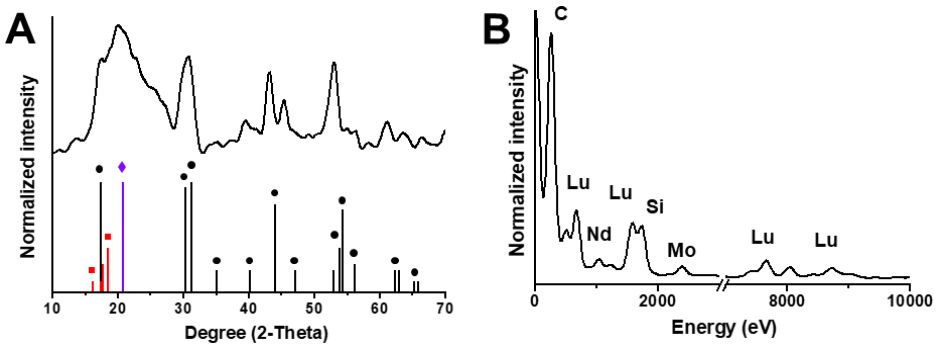

Supplementary Figure 2. Characterization of Ln-mSiMo. X-ray diffraction pattern (A) and energy-dispersive X-ray spectrum (B) of Ln-mSiMo. The black, violet, and red labels correspond to β-$NaLuF_4$ (JCPDS: 027-0726), amorphous SiO_2, and amorphous silicomolybdate.

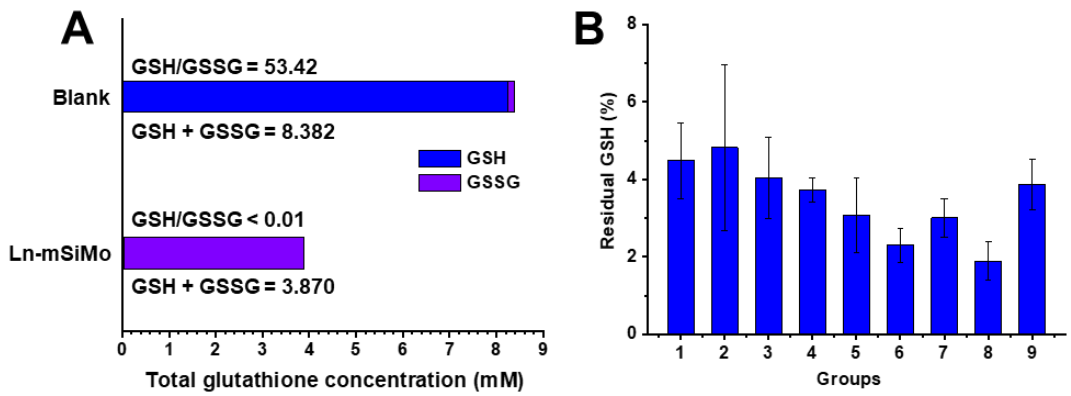

Supplementary Figure 3. Elimination of GSH by Ln-mSiMo. (A) GSH/GSSG ratio and total glutathione concentration before and after treated by Ln-mSiMo. (B) Residual GSH amount after treated by Ln-mSiMo with different initial GSH concentration. Data are represented as mean ± SD (n = 3).

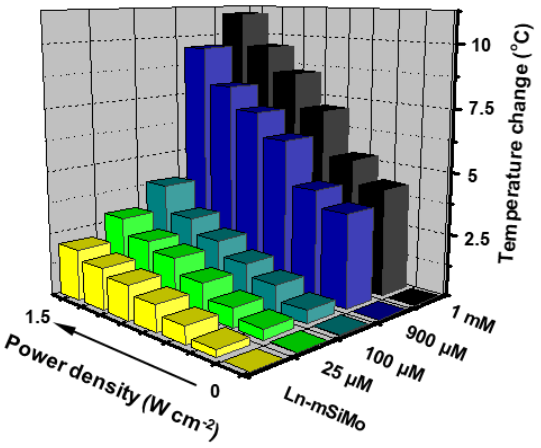

Supplementary Figure 4. Temperature change of Ln-mSiMo, reduced by different concentrations of GSH as a function of power density.

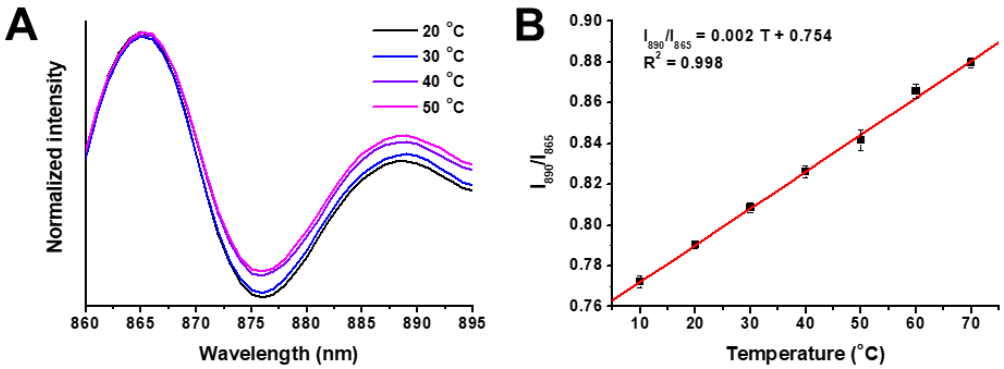

Supplementary Figure 5. Thermosensitive fluorescence of Nd^{3+} in Ln-mSiMo. (A) Fluorescence spectra of Ln-mSiMo at different temperatures by external heating. Peaks were normalized at 865 nm. (B) Plot of I_{890}/I_{865} ratio versus temperature, to calibrate the thermometric scale for Ln-mSiMo. Data are represented as mean ± SD (n = 3).

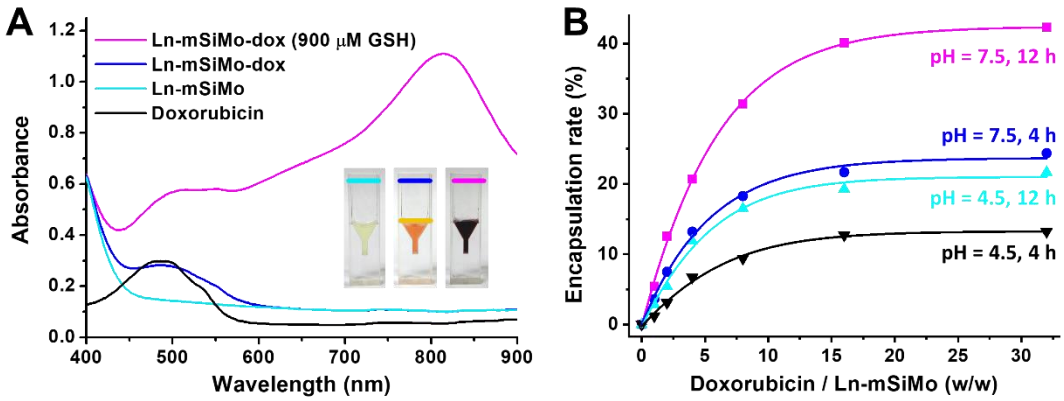

Supplementary Figure 6. Delivery of doxorubicin by Ln-mSiMo. (A) UV-vis-NIR spectra of Ln-mSiMo-dox reduced by 900 μM GSH, Ln-mSiMo-dox, Ln-mSiMo, and free doxorubicin. (B) Plots of loading ratio of doxorubicin onto Ln-mSiMo *vs* concentration of doxorubicin at different pH conditions and different time points.

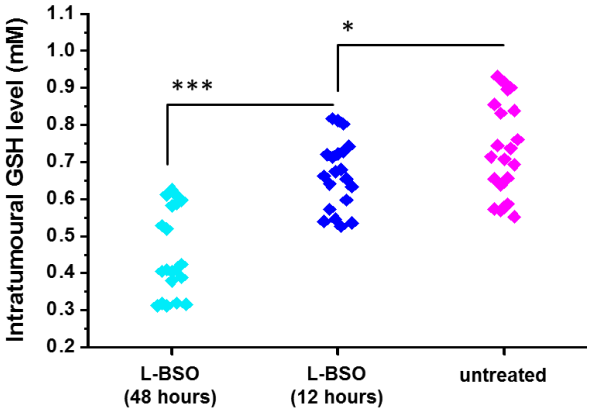

Supplementary Figure 7. Down-regulation of intratumoral GSH level by L-buthionine-sulfoximine (L-BSO). The intratumoral GSH level determined by a commercial GSH assay kit (Beyotime Biotechnology) after treatment with L-BSO, which is an irreversible inhibitor of γ-glutamylcysteine synthetase. Statistical significance was determined from one-way t tests. *$p < 0.05$, ***$p < 0.001$.

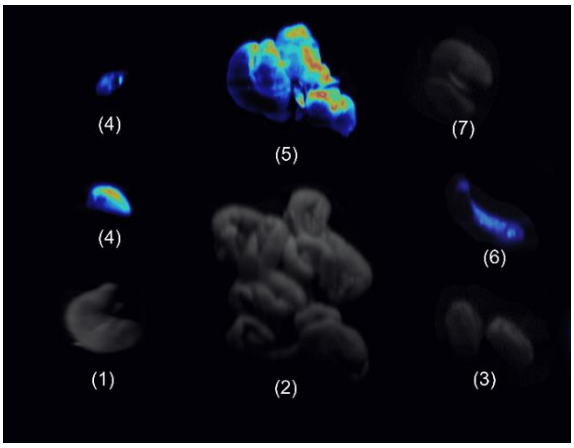

Supplementary Figure 8. NIR II fluorescence image of organs harvested from mice receiving a Ln-mSiMo injection. (1) Stomach; (2) intestine; (3) kidney; (4) tumors; (5) liver; (6) spleen; (7) lung.

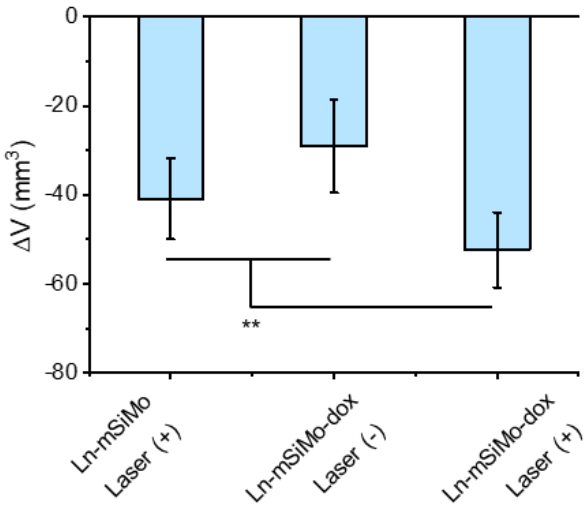

Supplementary Figure 9. Tumor size change of mice after receiving Ln-mSiMo-dox with laser irradiation. Mice receiving Ln-mSiMo with laser irradiation and Ln-mSiMo-dox without laser irradiation were used for comparison. Data are represented as mean ± SD (n = 10). Statistical significance was determined by one-way t tests. $^{**}p < 0.01$.

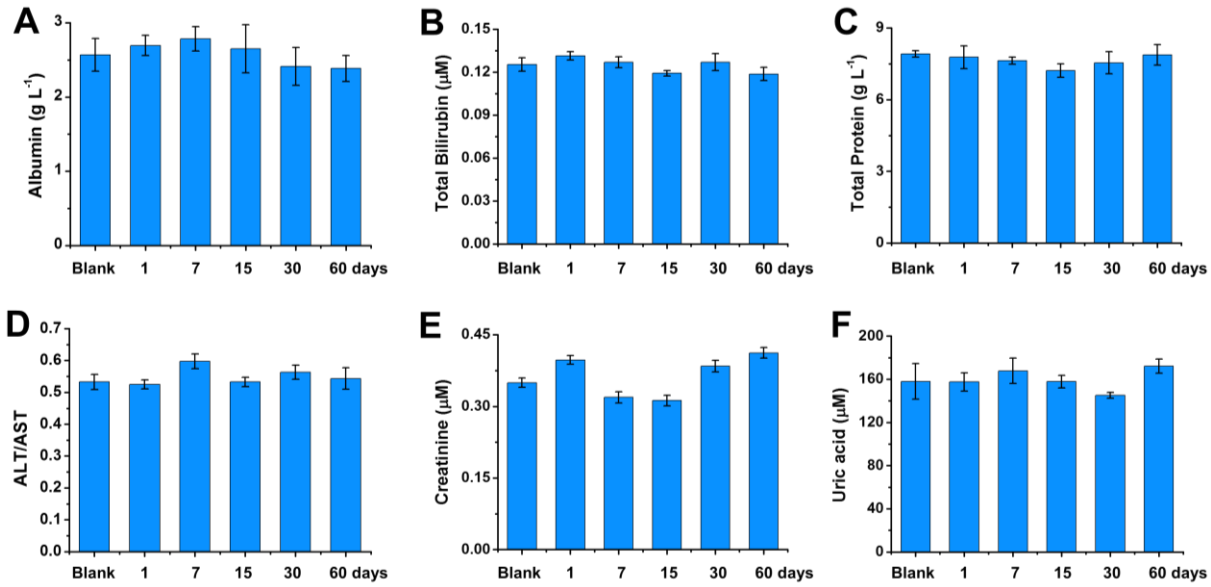

Supplementary Figure 10. Serology study of mice receiving Ln-mSiMo injection.

Serum biochemistry results, including albumin (a), total bilirubin (b), total protein (c), ALT/AST (d), creatinine (e), and uric acid (f), obtained from serum samples harvested from mice receiving Ln-mSiMo nanocomposites injection after 1, 7, 15, 30, and 60 days. ALT: alanine aminotransferase; AST: aspartate aminotransferase. Data are represented as mean ± SD (n = 3).

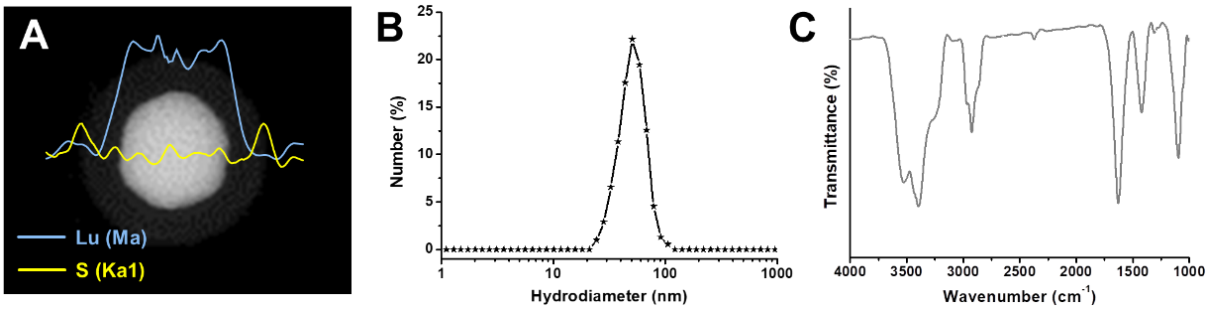

Supplementary Figure 11. Characterization of Ln-mSi-ICG. (A) Energy-dispersive X-ray line scan of a Ln-mSi-ICG signal. Hydrodiameter (B) and Fourier-transform infrared spectrum (C) of Ln-mSi-ICG.

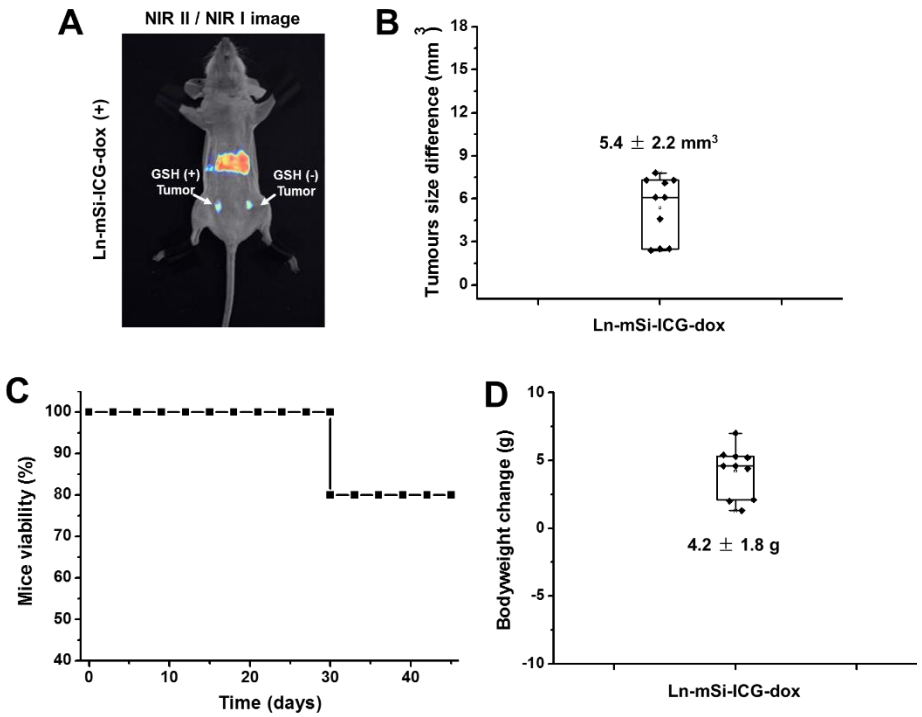

Supplementary Figure 12. Multi-tumor ablation by Ln-mSi-ICG *in vivo*. (A) NIR II/NIR I ratiometric fluorescence imaging of a mouse bearing a dual orthotopic breast tumor with different GSH levels. Difference between different tumors (B), viability (C), and bodyweight change (D) of mice after receiving Ln-mSi-ICG administration and uniform irradiation.

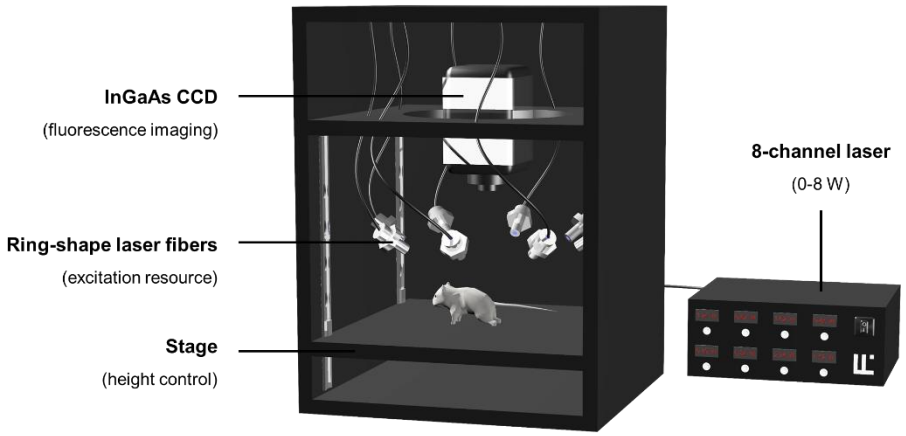

Supplementary Figure 13. Brief description of the ring-shape laser array. The laser array contained 8 laser fibers that were linked to one 8-channel laser (808 nm, output power 0-8 W), which was used as the excitation source for synergistic treatment. The positions of the laser fibers were fixed (holders not shown in the image), but the angle of fibers and size of laser spots could be modulated. By adjusting the output power independently, a non-uniform light field could be generated. The power density was quantified by a power meter. The mice were fixed on the stage during the treatment, which could be adjusted in height by an internal stage. For fluorescence imaging and establishment of irradiation prescription, an InGaAs CCD was installed at the top.

Supplementary Table 1. Tumor size of mice within non-uniform irradiation group for synergistic treatment *in vivo*. (unit of tumor size: mm^3)

Day	Tumor	1	2	3	4	5	6	7	8	9	10
0	Left	65.9	62.1	42.7	64.1	62.4	54.9	66.2	46.8	52.1	65.9
	Right	68.5	49.4	53.2	41.7	69.5	64.1	45.8	51.1	60.9	66
2	Left	54.4	55.4	34.1	52.5	47.7	35.7	57.1	30.5	40.4	51.9
	Right	41.2	40.5	48.3	28.6	64.2	54.9	33.6	42.5	42.2	49.8
5	Left	36.1	41.4	27.6	44.3	39.3	20.6	41.7	25.6	26.8	43
	Right	27.5	30.6	38.1	18.9	47.3	37.7	26.2	30.5	26.2	31.8
7	Left	19.4	31.8	22.6	23.9	30.1	15.3	24.4	14.7	13	30.8
	Right	20.1	16.8	24.8	12.5	28.6	22.4	14.7	20.1	16.9	20.7
10	Left	9.7	12.9	6.5	10.2	15	7.8	7	7.1	7.3	12.1
	Right	6.5	9.1	13.5	10.1	11.5	9.2	10.1	8.9	8.7	12.8
12	Left	1.7	0	0.7	2.4	3.6	0	1.1	0.4	0	4.5
	Right	1.4	3.7	2	5.7	3.5	3.4	3.3	2.6	0.2	4.3
Size difference		0.3	3.7	1.3	3.3	0.1	3.4	2.2	2.2	0.2	0.2

Supplementary Table 2. Tumor size of mice within uniform irradiation (high) group for synergistic treatment *in vivo*. (unit of tumor size: mm^3)

Day	Tumor	1	2	3	4	5	6	7	8	9	10
0	Left	47	43.3	47.7	41	68.2	62	50.1	50.2	42.1	68.5
	Right	52.7	63.1	65	65.8	56.3	43.5	47.2	59	67.2	44.2
2	Left	42.4	38.9	44	31.8	54.3	53.4	49.7	37.4	33	55.4
	Right	41.2	48	55.7	47	49	39.9	43.4	50.3	54.3	36.2
5	Left	35.2	35.7	32.1	27.2	37.4	41	40.8	25.4	28.6	37.2
	Right	32.8	40.8	49.7	34.8	36.5	34	33.8	36.7	39.8	30.5
7	Left	22.8	21.4	18.5	20	24	28.1	26.9	15.4	18.7	15.8
	Right	22.2	26.3	31	27	24.3	25.4	24.8	27.6	19.8	21
10	Left	14.1	14.8	8.3	11.8	14.2	16	16.3	8.9	7.6	8.2
	Right	10	12.1	17.3	14.6	9.3	10.2	13.5	15.8	10.9	12.6
12	Left	1.9	0.4	2.4	3.7	2.1	2.8	2.6	3.9	1.7	1.4
	Right	0.1	2.9	0.1	4.8	0	4	4.3	1.4	0.3	1.8
Size difference		0.3	1.8	2.5	2.3	1.1	2.1	1.2	1.7	2.5	1.4

Supplementary Table 3. Tumor size of mice within uniform irradiation (low) group for synergistic treatment *in vivo*. (unit of tumor size: mm^3)

Day	Tumor	1	2	3	4	5	6	7	8	9	10
0	Left	52.4	42.9	59.1	44.3	62.6	45.7	54.9	54.1	47.4	42.5
	Right	50.5	58.9	56.4	64.7	56	54.4	46.9	60.4	61.6	68.4
2	Left	48	48.9	42.4	51.2	59	56.9	54.2	47.7	34.7	59.9
	Right	45.1	65.3	50.6	55.8	45.6	60.6	41	50.4	52.6	72.1
5	Left	45.9	61.7	29.2	60.6	35.2	76.1	53.5	33.9	21.3	59.4
	Right	38.6	73.4	42	58.3	45.5	69.4	36.6	37.6	30.1	65.6
7	Left	37.8	73.5	20.2	70.9	25.4	89.3	46.5	19.8	14	63.1
	Right	30.7	86.9	32.5	61.7	39	72.2	38.9	27.6	23.3	66
10	Left	29.4	84.9	12	74.3	18.3	95.7	37.3	7.6	9.1	67.1
	Right	32.1	89.7	24.7	64.4	29.1	83.4	31.6	20.2	14.4	69
12	Left	21.7	96.4	3.3	76.4	12.2	102.1	30.4	2.1	0.8	77.2
	Right	35.2	80.1	17.6	72.7	21	87.4	33	13.2	5.8	69.7
Size difference		13.5	16.3	14.3	3.7	8.8	14.7	2.6	11.1	5	7.5

References

[1] Y. X. Liu, Q. W. Guo, X. J. Zhu, W. Feng, L. Wang, L. Y. Ma, G. Zhang, J. Zhou, F. Y. Li, *Adv. Funct. Mater.* **2016**, *26*, 5120-5130.

[2] Y. X. Liu, Q. Jia, X. J. Zhai, F. Mao, A. Q. Jiang, J. Zhou, *Chem. Sci.* **2019**, *10*, 1193-1200.

[3] W. Stober, A. Fink, E. Bohn, *J. Colloid. Interface Sci.* **1968**, *26*, 62-69.

[4] J. E. Liebmann, S. M. Hahn, J. A. Cook, C. Lipschultz, J. B. Mitchell, D. C. Kaufman, *Cancer Res.* **1993**, *53*, 2066-2070.